

doi.org/10.1002/minf.202100231

# Development and Evaluation of Peptidomimetic Compounds against SARS-CoV-2 Spike Protein: An *in silico* and *in vitro* Study

Omid Zarei<sup>+</sup>,<sup>[a]</sup> Hannah Kleine-Weber<sup>+</sup>,<sup>[b, c]</sup> Markus Hoffmann,<sup>[b, c]</sup> and Maryam Hamzeh-Mivehroud<sup>\*,[d, e]</sup>

**Abstract: Background:** Coronavirus disease 2019 (COVID-19) as global pandemic disease has been adversely affecting public health and social life with considerable loss of human life worldwide. Therefore, there is an urgent need for developing novel therapeutics to combat COVID-19. The causative agent of COVID-19 is SARS-CoV-2 which targets human angiotensin converting enzyme 2 (ACE2) as cellular receptor via its spike (S) protein. In this context, interfering with the binding of SARS-CoV-2 S protein to target molecules could provide a promising strategy to find novel therapeutic agents against SARS-CoV-2. The purpose of the current study was to identify potential peptidomimetics against S protein with a combination of structure-based

virtual screening methods and *in vitro* assays. **Methods:** The candidates were inspected in terms of ADME properties, drug-likeness, as well as toxicity profiles. Additionally, molecular docking and dynamics simulations were performed to predict binding of the studied ligands to spike protein. **Results:** Biological evaluation of the compounds revealed that PM2 molecule exhibits some antiviral activity. **Conclusion:** In summary, this study highlights the importance of combining *in silico* and *in vitro* techniques in order to identify antiviral compound to tackle COVID-19 and presents a new scaffold that may be structurally optimized for improved antiviral activity.

**Keywords:** COVID-19 · SARS-CoV-2 · Spike · peptidomimetics · virtual screening

## 1 Introduction

Coronavirus disease 2019 (COVID-19) is a novel emerging disease that was first detected in winter 2019 in the city of Wuhan, China, and since then has expanded into a pandemic.<sup>[1]</sup> As of January 1, 2022, 290 million laboratory confirmed infections with over 5.4 million deaths related to COVID-19 have been recorded (<https://www.worldometers.info/coronavirus/>). High transmissibility in combination with the lack of effective therapeutics and struggle to establish global vaccination program has allowed COVID-19 to become a public health threat world-wide.<sup>[2]</sup> The causative agent of COVID-19 was identified to be a novel coronavirus and has been termed SARS-CoV-2 and as all members of the *Coronaviridae* family, SARS-CoV-2 is an enveloped virus with a non-segmented, single-stranded RNA genome of positive polarity (+ ssRNA).<sup>[3]</sup> SARS-CoV-2 transmission usually occurs via tiny respiratory droplets (e.g., aerosols) but also other transmission routes involving contaminated surfaces<sup>[4]</sup> as well as oral fecal and mother to fetus transmissions have been reported.<sup>[5]</sup> A wide range of symptoms from fever, sore throat, dry cough, fatigue, and dyspnea to gastrointestinal, cutaneous and ocular manifestations have been reported for mild to severe forms of COVID-19.<sup>[6]</sup> Although it has been shown that some of infected individuals remain asymptomatic.<sup>[7]</sup>

From the beginning of the COVID-19 outbreak, different experimentally combinations of therapeutic agents have

been utilized to reduce the disease severity and mortality in hospitalized/non hospitalized patients,<sup>[8]</sup> but to date, there is no specific drug available against SARS-CoV-2 with strong clinical benefit on the course of disease, emphasizing the necessity of developing novel drugs for the treatment of COVID-19 patients.

The use of computational approaches in the drug discovery and development process is inevitable as these approaches hold the promise of making significant contri-

[a] O. Zarei<sup>+</sup>

Cellular and Molecular Research Center, Research Institute for Health Development, Kurdistan University of Medical Sciences, Sanandaj, Iran

[b] H. Kleine-Weber,<sup>+</sup> M. Hoffmann

Infection Biology Unit, German Primate Center – Leibniz Institute for Primate Research, Göttingen, Germany

[c] H. Kleine-Weber,<sup>+</sup> M. Hoffmann

Faculty of Biology and Psychology, Georg-August-University Göttingen, Göttingen, Germany

[d] Ph. D. M. Hamzeh-Mivehroud

Biotechnology Research Center and School of Pharmacy, Tabriz University of Medical Sciences, Tabriz, Iran

E-mail: hamzehm@tbzmed.ac.ir

maryam\_h\_7860@yahoo.com

[e] Ph. D. M. Hamzeh-Mivehroud

School of Pharmacy, Tabriz University of Medical Sciences, Tabriz, Iran

[<sup>+</sup>] These authors have equally contribution in this work.

butions to this process in a time- and cost-affordable manner. In this context, virtual screening as a computationally driven tool can fulfill a gap between theory and experiment by identification of novel inhibitors against targets of interest.<sup>[5b]</sup> Up to now, plenty of computational studies have been documented aiming to find SARS-CoV-2 inhibitors especially against the viral spike (S) glycoprotein using drug repurposing strategy.<sup>[9]</sup> The S protein is a surface glycoprotein of SARS-CoV-2 containing 1273 amino acids, consisting of a signal peptide (Met<sup>1</sup> to Ser<sup>13</sup>), S1 subunit (Gln<sup>14</sup> to Arg<sup>685</sup>), and S2 subunit (Ser<sup>686</sup> to Thr<sup>1273</sup>).<sup>[10]</sup> The interaction of SARS-CoV-2 S protein with its cellular receptor, angiotensin converting enzyme 2 (ACE2), is considered to be the key step required for viral entry into a cell.<sup>[11]</sup> The receptor binding domain (RBD) located within the globular head of the S protein is a crucial domain as it contains the amino acid residues that directly engage ACE2.<sup>[11a]</sup> Therefore, interfering with S protein binding to ACE2 is a powerful way to block SARS-CoV-2 infection and identification of agents with such properties a promising strategy.

The aim of this study was to identify the potential peptidomimetic compounds against SARS-CoV-2 S protein using a structure-based, virtual screening method based on the molecular structure of ACE2. The identified molecules were subjected to *in vitro* assays to investigate their ability to inhibit SARS-CoV-2 S protein-mediated cell entry in a pseudotype virus surrogate model.

## 2 Materials and Methods

### 2.1 Computational Studies

#### 2.1.1 Molecular Modeling

A homology-based model structure for receptor binding domain (RBD) of SARS-CoV-2 S protein in complex with human ACE2 was generated based on the experimentally determined 3D structure of SARS-CoV.<sup>[12]</sup> The modeled structure was then used as guide structure for virtual screening procedure.

#### 2.1.2 Structure-based Virtual Screening

Structure-based virtual screening was performed using a web-oriented platform known as "pep:MMs:MIMIC" using a library of ~17 million multi conformers obtained from chemical structures available in MMsINC<sup>®</sup> database.<sup>[13]</sup> The screening process was carried out by introducing the 3D-pharmacophore based on the identified key residues of the ACE2 involved in the interaction with the S protein including Lys<sup>31</sup>, Glu<sup>35</sup>, Asp<sup>38</sup>, and Lys<sup>353</sup>.<sup>[12]</sup> Different scoring methods including ultrafast shape recognition (USR) and pharmacophoric fingerprint similarity (PFS) or combination

of the methods (so called hybrid method) implemented in pep:MMs:MIMIC platform were applied to rank the top 200 peptidomimetics candidates.

#### 2.1.3 Drug-likeness, ADME Profiling, and Toxicity Risk Assessment

The top ranked peptidomimetics obtained from MMsINC<sup>®</sup> database were inspected in terms of drug likeness, pharmacokinetic, and physicochemical properties SwissADME webserver (<http://www.swissadme.ch/>).<sup>[14]</sup> A set of drug-likeness criteria based on Lipinski, Veber, Egan, Muegge, and Ghose<sup>[15]</sup> were used to filter the retrieved compounds. The peptidomimetic candidates that successfully passed the drug-likeness filters were kept for further inspections. Moreover, ADME (absorption, distribution, metabolism, and elimination) profile of the molecules were computationally predicted in SwissADME webserver. In addition, a variety of physicochemical parameters as well as and medicinal chemistry friendliness properties were also calculated using this web tool. In order to estimate the binding affinity profile of the peptidomimetic compounds to off-target proteins, OpenVirtualToxLab program (version 5.8) was utilized. In this platform, a thermodynamic dependant parameter called toxic potential (TP) was estimated using flexible docking of the given candidate molecules to off-target proteins by applying 4D Boltzmann scoring criterion.<sup>[16]</sup> The calculated TP values ranged from zero to unity in which the lower values of this parameter indicate the lower potential to be toxic.

For toxicity evaluation, OpenVirtualToxLab (version 5.8) was used for anticipating toxic potential (TP) by providing estimation of binding affinity profile of the candidate molecules to off-target proteins including nuclear receptors (AR, ER $\alpha$ , ER $\beta$ , GR, MR, PR, LXR, PPAR $\gamma$ , TR $\alpha$ , and TR $\beta$ ), cytochrome P450 enzyme family (1A2, 2C9, 2D6, 3A4), a cytosolic transcription factor (AhR) and a potassium ion channel (hERG). Then, the selected candidate molecules were introduced to the next step of analyses.

#### 2.1.4 Molecular Docking

The 3D structures of the selected peptidomimetic compounds were obtained from pep:MMs:MIMIC and subjected to energy minimization using MM+ force field based on Polack-Ribiere algorithm implemented in Hyperchem software (version 8.0.8). Then the structures were fully optimized using *ab initio* method at the restricted Hartree-Fock (RHF) level of theory with small 3-21G basis set.<sup>[17]</sup>

Molecular docking of the selected compounds into the homology-based model of SARS-CoV-2 spike protein was carried out using GOLD program (version 5.0, CCDC, Cambridge, UK). For this purpose, geometric center of the important binding involved residues of SARS-CoV-2 S

protein (i.e., Leu<sup>455</sup>, Phe<sup>486</sup>, Gln<sup>493</sup>, Ser<sup>494</sup>, Asn<sup>501</sup>) was determined and set as the center of binding site considering all atoms within a radius of 10 Å. Semiflexible docking was considered for molecular docking calculations in which the side chains of amino acids were allowed to be flexible while the backbone atoms were kept rigid. Subsequently, the best pose of docked ligands was selected based on the ChemPLP scoring function.<sup>[18]</sup> Then, the complexes were analyzed in terms of interaction mode by PyMol and LigPlot programs.<sup>[19]</sup> Furthermore, molecular docking of selected peptidomimetic compounds into the resolved crystal structure of the spike protein (PDB ID: 6 MO J)<sup>[11a]</sup> was also performed based on the above mentioned protocol and the obtained results were compared with docking experiment based on homology-model of spike protein.

### 2.1.5 Molecular Dynamics (MD) Simulation and Binding Free Energy Calculation

Top-ranked docking pose in complex with spike protein on the basis of ChemPLP fitness function was processed for molecular dynamics simulation analysis using AMBER package.<sup>[20]</sup> To this end, AMBER usable coordinate files were generated via *LEaP* module using Amber99SB force-field. Then, the correct number of counter ions (i.e. Na<sup>+</sup> or Cl<sup>-</sup>) were added for neutralizing the total charge of the system followed by immersing the system into a rectangular box of explicit TIP3P water molecules with the buffering distances of 12 Å outside the solute on all sides. The solvated system was subjected to energy minimization by 500 steps of steepest descent followed by 500 steps of conjugated gradient using *Sander* module of AMBER package. Then, the temperature of the system was gradually raised during a 50 ps heating step from 0 to 300 K with subsequent 50 ps of density equilibration and 500 ps of constant pressure equilibration under temperature of 300 K and pressure of 1 atm with a time step of 2 fs. All bond lengths involving hydrogen atoms were constrained by applying SHAKE algorithm. Finally, a 20 ns MD simulation was conducted using the particle mesh Ewald (PME) method for computing the long-range electrostatic interactions. All the calculations were performed under periodic boundary conditions without utilizing any constraint either on the protein or the ligand molecules. MD simulation trajectory was obtained by keeping the coordinates every 10 ps. Following the MD simulation, post-processing the simulation trajectory was carried out for calculation of binding free energy on the inhibitor-protein complex. For this purpose, the snapshots were extracted from the trajectory with an interval of 10 ps. The values of the dielectric constant were set to 1.0 and 80 for the interior solute and the surrounding solvent, respectively. The binding free energy was calculated using molecular mechanics Poisson–Boltzmann surface area (MM-PBSA)/generalized Born–surface area (GBSA) methods implemented in the AMBER package.<sup>[20b,21]</sup> The ligand-protein

interaction energy was obtained based on the averaging over the extracted snapshots energies without considering the water molecules and counter ions. In this study, the entropy term of the solute was ignored in the calculations assuming similar entropy contribution for the complexes to the binding free energy.

Binding free energy ( $\Delta G_{\text{bind}}$ ) is calculated according to the following equation:

$$\Delta G_{\text{bind}} = G_{\text{water}(\text{complex})} - G_{\text{water}(\text{protein})} - G_{\text{water}(\text{ligand})}$$

In this equation,  $G_{\text{water}(\text{complex})}$ ,  $G_{\text{water}(\text{protein})}$  and  $G_{\text{water}(\text{ligand})}$  denote the free energies of the complex, protein, and ligand, respectively. Free energy for each species is calculated as follows:

$$G = E_{\text{gas}} + \Delta G_{\text{solvation}} - TS$$

$$\Delta G_{\text{solvation}} = \Delta G_{\text{polar}} + \Delta G_{\text{non-polar}}$$

$$E_{\text{gas}} = E_{\text{int}} + E_{\text{vdw}} + E_{\text{elec}}$$

$$E_{\text{int}} = E_{\text{bond}} + E_{\text{angle}} + E_{\text{tors}}$$

where  $E_{\text{gas}}$  as the standard force-field energy is composed of internal energy ( $E_{\text{int}}$ ) in the gas phase as well as non-covalent van der Waals ( $E_{\text{vdw}}$ ) and electrostatic ( $E_{\text{elec}}$ ) energies.  $E_{\text{bond}}$ ,  $E_{\text{angle}}$ , and  $E_{\text{tors}}$  demonstrate the contributions to the internal energy arisen from vibrations of the bonds, angle, and torsion angle from their equilibrium values, respectively.  $\Delta G_{\text{solvation}}$  refers to solvation free energy which is comprised of  $\Delta G_{\text{polar}}$  and  $\Delta G_{\text{non-polar}}$  as polar and non-polar contributions to the solvation free energy, respectively. Poisson-Boltzmann or Generalized Born model are used for calculation of polar contribution whereas non-polar contribution is obtained by computation of solvent accessible surface area (SASA) using the linear combinations of pairwise overlaps (LCPO) method.<sup>[22]</sup>

## 2.2 Biological Evaluation

The *in silico*-based selected compounds PM1 (Cat. #: MolPort-007-680-453) and PM2 (Cat. #: MolPort-007-944-288) were purchased from MolPort (Latvia) as lyophilized powder and were dissolved in DMSO (stock: 10 mM). Similarly, camostat mesylate, a serine-protease inhibitor that is well-known for its ability to inhibit SARS-CoV-2 entry into Calu-3 cells,<sup>[23]</sup> was purchased from Sigma-Aldrich (Cat. #: SML0057) and dissolved in DMSO (stock: 10 mM). The compounds were further diluted in culture medium in order to obtain 10-fold serial dilutions, ranging from 0.01 nM to 100 μM. The cell lines Vero (African green monkey kidney cells, kindly provided by Andrea Maisner) and Calu-3 (Human lung cells, kindly provided by Stephan Ludwig) were used as target cells. Vero cells are a standard cell line

to investigate different viruses and are highly susceptible to coronaviruses. However, they are not the best model for human infections by coronaviruses. Therefore, we included the human lung cell line Calu-3 as a model that is closer to the *in vivo* situation. For the experiment, first medium containing the respective compound concentration (or medium without compound = control) was added to the cells and incubated for 30 minutes before viral pseudotype vectors bearing either SARS-CoV-2 S protein (codon-optimized, based on isolate hCoV-19/Wuhan/Hu-1/2019; GISAID: EPI\_ISL\_402125) or vesicular stomatitis virus glycoprotein (VSV-G) were added on top. Pseudotype vectors were generated based on a previously published protocol using a replication-defective vesicular stomatitis virus encoding firefly luciferase, VSV\* $\Delta$ G-fLuc (kindly provided by Gert Zimmer).<sup>[24]</sup> Following inoculation with pseudotype vectors, cells were incubated for 16 h at 37 °C and 5% CO<sub>2</sub>, before viral entry was investigated by quantifying virus-encoded luciferase activity. For this, cells were lysed with Cell Culture Lysis Reagent (Promega) for 30 min at room temperature. Next, lysates were transferred in white 96-well plates and firefly luciferase substrate (Beetle-Juice, PJK) was added before luminescence was measured using a Hidex Sense plate luminometer (Hidex).

### 3 Results and Discussion

The lack of effective drugs to inhibit SARS-CoV-2 and treat infected individuals is a major obstacle in the fight against the COVID-19 pandemic and calls for the development of novel therapeutic strategies.<sup>[25]</sup> In the current study, a combination of *in silico* and *in vitro* studies was applied for finding peptidomimetic compounds against the spike glycoprotein of SARS-CoV-2. Figure 1 demonstrates the overview of workflow utilized for the virtual screening procedure. First, four amino acids of ACE2 including Lys<sup>31</sup>, Glu<sup>35</sup>, Asp<sup>38</sup>, and Lys<sup>353</sup> as the proposed involved residues in the interaction with SARS-CoV-2 S protein<sup>[12]</sup> were used as input data for screening the peptidomimetic compounds in the chemical space of MMsINC<sup>®</sup> database.

Among the various scoring metrics implemented in pep:MMs:MIMIC platform, scoring methods such as shape and pharmacophoric similarity methods as well as hybrid methods (i.e., 60% pharmacophoric and 40% shape similarity) were applied for filtering the peptidomimetic library. Analyzing the results showed that only the candidates based on shape similarity scoring metric showed a desirable score (score > 0.5). Therefore, the top 200 ranked peptidomimetics obtained using this scoring function were selected for further analyses in terms of drug likeness and pharmacokinetic properties. For this purpose, the retrieved compounds were analyzed using the SwissADME webserver.<sup>[14]</sup> Based on drug-likeness and ADME properties, two peptidomimetic candidates (called as PM1 and PM2) were selected for further analysis. The structure, physico-

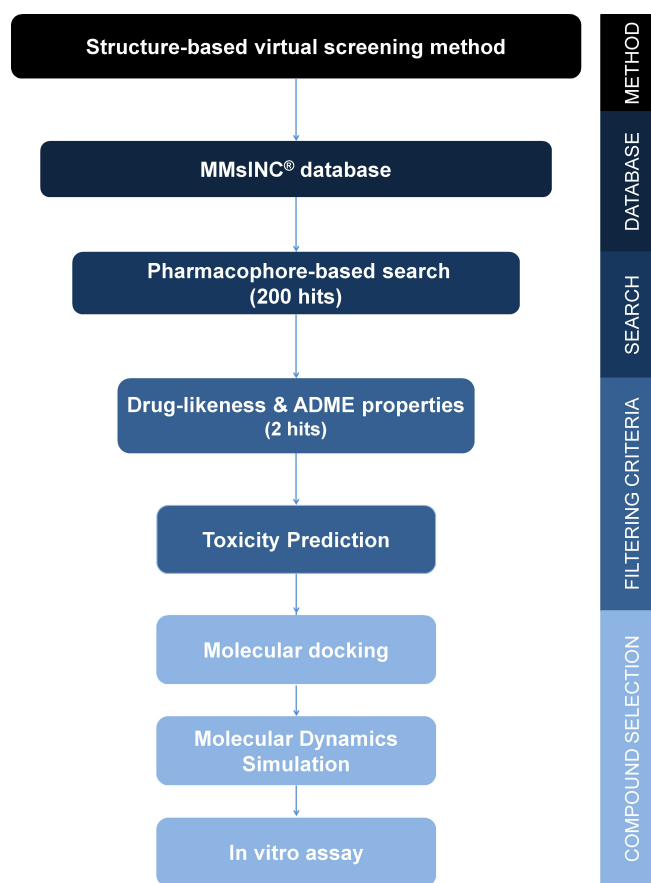


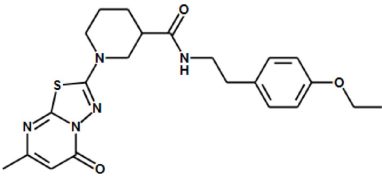
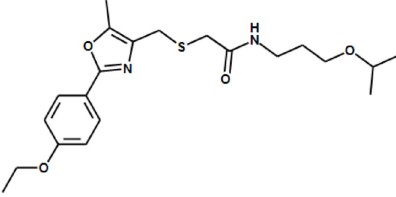
**Figure 1.** Overview of workflow used for virtual screening procedure.

chemical, pharmacokinetic, and drug likeness properties of the two selected compounds are shown in Table 1.

For estimation of toxic potential of the candidate molecules, OpenVirtualToxLab program was used in which automated and flexible molecular docking in conjunction with multi-dimensional quantitative structure–activity relationship (QSAR) are applied.<sup>[16b]</sup> In this approach endocrine and metabolic disruption as well as some aspects of carcinogenicity and cardiotoxicity are predicted using binding affinities of the given candidate molecules towards target proteins which are responsible for triggering adverse effect. The results of toxicity alert are presented as a thermodynamic-dependant parameter known as toxic potential (TP) ranging from zero to unity, which is classified in five categories (i.e., 0, I, II, III, and IV). The lower value of TP in the scale of toxicity alert indicates the lower potential of toxicity. Table 2 provides the result of toxicity risk assessment for the peptidomimetic candidates PM1 and PM2 indicative of possible safety of the selected compounds in terms of toxicity scale.

In the next step, in order to determine the binding mode of interaction between the selected compounds and homology-based model of spike protein, molecular docking

**Table 1.** Physicochemical, pharmacokinetic, drug-likeness and medicinal chemistry properties of lead compounds

Molecular Descriptor	PM1	PM2
Structures		
Physicochemical Properties		
Formula	C <sub>22</sub> H <sub>27</sub> N <sub>5</sub> O <sub>3</sub> S	C <sub>21</sub> H <sub>30</sub> N <sub>2</sub> O <sub>4</sub> S
Molecular weight	441.55 g/mol	406.54 g/mol
Num. rotatable bonds	8	13
Num. H-bond acceptors	5	5
Num. H-bond donors	1	1
Molar Refractivity	124.76	113.30
TPSA	117.07 Å <sup>2</sup>	98.89 Å <sup>2</sup>
Pharmacokinetic properties		
GI absorption	High	High
BBB permeant	No	No
P-gp substrate	Yes	No
CYP1A2 inhibitor	No	No
CYP2C19 inhibitor	Yes	No
CYP2C9 inhibitor	Yes	No
CYP2D6 inhibitor	Yes	Yes
CYP3A4 inhibitor	Yes	Yes
Log K <sub>p</sub> (skin permeation)	-7.09 cm/s	-6.24 cm/s
Drug likeness		
Lipinski	Yes	Yes
Ghose <sup>a</sup>	Yes	Yes
Veber <sup>b</sup>	Yes	No
Egan <sup>c</sup>	Yes	Yes
Muegge <sup>d</sup>	Yes	Yes
PAINS	No	No
Brenks	No	No
Bioavailability Score	0.55	0.55

<sup>a</sup> Ghose filter: 160 ≤ MW ≤ 480; -0.4 ≤ WLOGP ≤ 5.6; 40 ≤ MR ≤ 130; 20 ≤ atoms ≤ 70.

<sup>b</sup> Veber filter: Rotatable bonds ≤ 10; TPSA ≤ 140.

<sup>c</sup> Egan filter: WLOGP ≤ 5.88; TPSA ≤ 131.6.

<sup>d</sup> Muegge: 200 ≤ MW ≤ 600; -2 ≤ XLOGP ≤ 5; TPSA ≤ 150; Num. rings ≤ 7; No of carbons > 4; Num. heteroatoms > 1; Num. rotatable bonds ≤ 15; Num. H-bond acceptors ≤ 10; and Num. H-bond donors ≤ 5.

analysis was conducted. Figure 2 illustrates the mode of interaction between the peptidomimetic candidates and the modeled structure of spike protein. For the docking experiment, ChemPLP scoring function was used to rank the docking solutions of the candidate molecules and the population size, number of operations and number of islands were set to 100, 100,000 and 5, respectively. Analysis of molecular docking results demonstrates that both of candidates, PM1 and PM2, establish hydrogen bonds and hydrophobic interactions with SARS-CoV-2 S protein. The identified interactions for PM1 include three hydrogen bonds and hydrophobic interactions. Tyr<sup>453</sup>, Gln<sup>493</sup>, and Gly<sup>496</sup> are engaged in the hydrogen bond with nitrogen (i.e., N5), sulfur, and oxygen atoms of thiadiazolo pyrimidin-5-one ring of PM1, respectively. PM1 is also involved in

hydrophobic interactions with residues Arg<sup>403</sup>, Glu<sup>406</sup>, Tyr<sup>449</sup>, Ser<sup>494</sup>, and Tyr<sup>495</sup> from SARS-CoV-2 S protein. In the case of PM2, similar interactions were observed: Lys<sup>417</sup> of S protein forms an H-bond with the oxygen adjacent to isopropyl at the endmost of the molecule. Additionally, two hydrogen bonds are observed between Tyr<sup>449</sup> and Gly<sup>496</sup> of S protein and oxygen atoms of ethoxy and oxazole moieties. Similar to PM1, hydrophobic interactions are also predicted in the complex of PM2-SARS-CoV-2 S protein (see Figure 2). As the homology-based model of spike protein is too similar to the solved crystal structure of spike protein (PDB ID: 6MOJ) deduced from the lower RMSD value of the backbone  $\alpha$ -carbon atoms (i.e. 0.5 Å), we decided to perform molecular docking of the selected peptidomimetics into the solved structure of spike protein and compare the results with

**Table 2.** *In silico* Toxicity evaluation of investigated peptidomimetic compounds. The calculated binding affinities ( $IC_{50}$ , Molar) for selected candidates against all 16 target proteins as well as toxic potential using VirtualToxLab are shown.

Molecule	Toxic Potential	AR	AhR	CYP1A2	CYP2C9	CYP2D6	CYP3A4	ER $\alpha$	ER $\beta$	GR	hERG	LXR	MR	PPAR $\gamma$	PR	TR $\alpha$	TR $\beta$
PM1	0.323	9.39E-06	NB	NB	NB	NB	NB	NB	NB	4.47E-06	NB	8.09E-05	1.66E-05	NB	4.14E-06	1.82E-05	NB
PM2	0.332	NB	NB	NB	NB	NB	NB	NB	NB	NB	4.66E-06	1.19E-05	NB	2.98E-05	NB	NB	NB

AR: Androgen receptor; AhR: Aryl hydrocarbon receptor; ER $\alpha$ : Estrogen receptor  $\alpha$ ; ER $\beta$ : Estrogen receptor  $\beta$ ; GR: Glucocorticoid receptor; hERG:

LXR: Liver X receptor; MR: Mineralocorticoid receptor; PR: Progesterone receptor; TR $\alpha$ : Thyroid receptor  $\alpha$ ; TR $\beta$ : Thyroid receptor  $\beta$ ; NB: Not binding.

TP is a measure of toxic potential derived from normalized binding affinities in respect to series of proteins with known adverse effects. Toxic alerts are defined as:

Class 0:  $TP \leq 0.3$  (none);  $0.3 < TP \leq 0.4$  (low);  $0.4 < TP \leq 0.5$  (moderate)

Class I:  $0.5 < TP \leq 0.6$  (elevated)

Class II:  $0.6 < TP \leq 0.7$  (high)

Class III:  $0.7 < TP \leq 0.8$  (Very high)

Class IV:  $> 0.8$  (Extreme)

docking prediction based on the homology-model of spike protein. Analyses of the results demonstrated that the predicted interactions observed for PM1 and PM2 are in agreement with those obtained based on homology-model of spike protein. Figure 3 shows the superimposed docking poses of the PM1 and PM2 bound into the modeled and crystal structures of the spike protein. As it can be seen in Figure 3, the conformation and orientation of the docked compounds in complex with both target structures are mostly identical.

The predicted interactions observed for the peptidomimetic compounds in complex with spike protein are identical to some extent with several previously published reports. In a study by Xiong et al, two novel inhibitors namely DC-RA016 and DC-RA052 were introduced as promising hits for blocking the interaction between SARS-CoV-2 S-RBD and ACE2. Biological evaluations of these molecules showed moderate antiviral activity against spike protein. The results of docking study conducted for these inhibitors demonstrated that some of residues such as Arg<sup>403</sup>, Glu<sup>406</sup>, Gln<sup>409</sup>, Lys<sup>417</sup>, and Gly<sup>496</sup> from spike protein are involved in the interactions with the identified molecules which are similar to the interactions observed in this study.<sup>[26]</sup> In other study, virtual screening of antiviral library extracted from the Asinex database was conducted and three compounds were identified as potential compounds against spike protein. Docking analysis of these molecules in complex with spike protein using GOLD program revealed that some residues of SARS-CoV-2 spike protein (like Arg<sup>403</sup>, Lys<sup>417</sup>, Tyr<sup>495</sup>, and Gly<sup>496</sup>) were involved in the interactions with the candidate molecules similar to those interactions observed in this study.<sup>[27]</sup> The other *in silico* investigation was aimed to design a peptide-based inhibitor named Mod13AApi with the potential to interfere with the attachment of spike protein of SARS-CoV-2 and its variants to ACE2. In this work, by employing molecular docking experiment, some similar interactions were also predicted for this tridecapeptide in complex with spike protein and its variants like the interactions anticipated for our study.<sup>[28]</sup> In 2021, Acharya and colleagues reported a study in which two potential compounds (called MU-UNMC-1 and MU-UNMC-2) as entry inhibitors for SARS-CoV-2 and its variants were discovered using virtual screening technique. These molecules were experimentally evaluated in a live SARS-CoV-2 infection assays. The results exhibited that both molecules demonstrated antiviral activity in micromolar range. Following the docking analysis conducted for these compounds, some interactions were also observed for residues located at the interface of spike protein with the identified molecules similar to those observed in our study.<sup>[29]</sup>

None of the predicted residues of spike protein engaged in the interactions with PM1 and PM2 are mutated in the known SARS-CoV-2 variants including Alpha (B.1.1.7), Beta (B.1.351), Gamma (P.1), Kappa (B.1.617.1), Delta (B.1.617.2), Delta+ (B.1.617.3), and Omicron ((B.1.1.529) variants, with

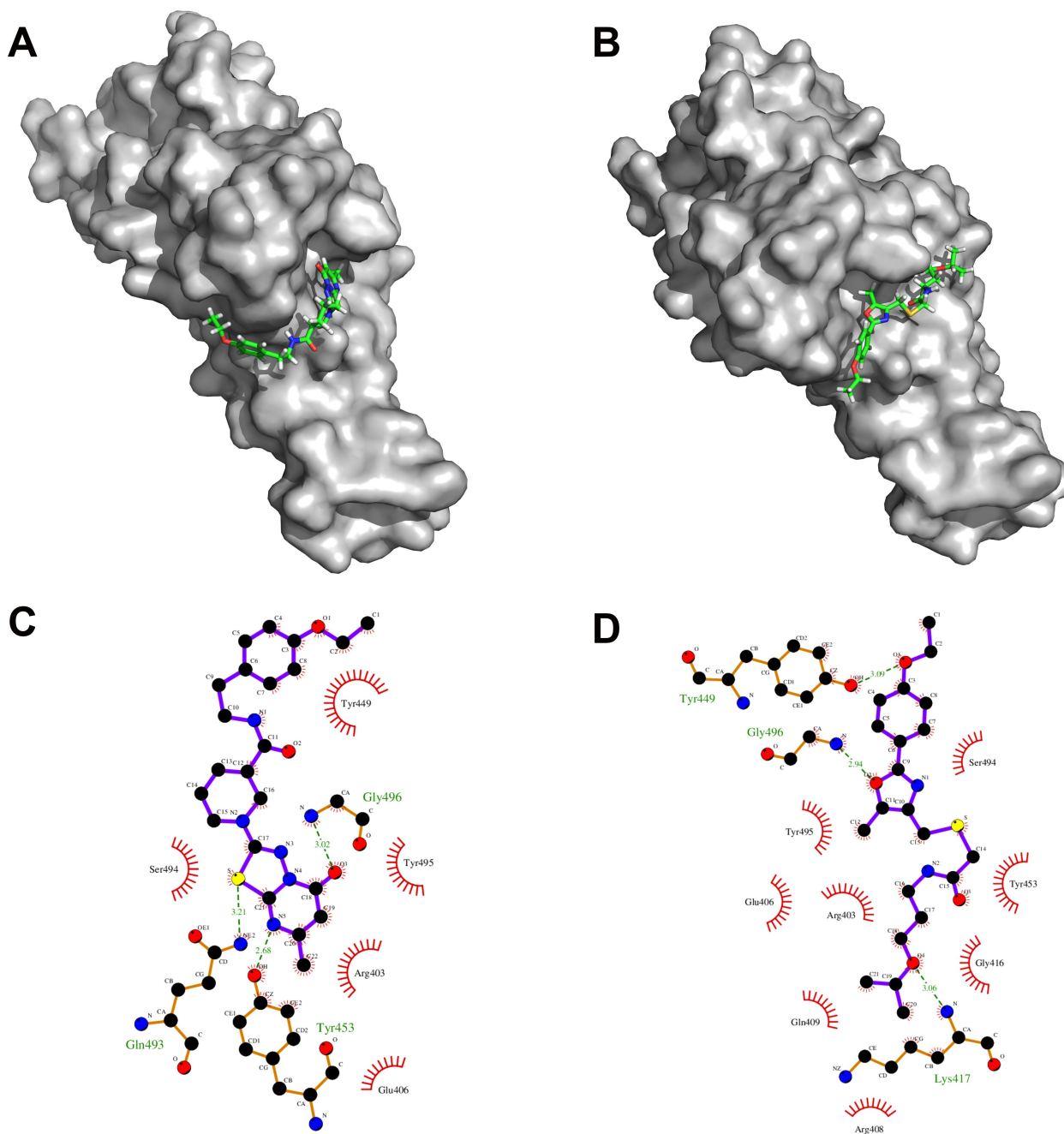


**Figure 2.** Three-dimensional (3D) representation of compounds PM1 and PM2 (Panels A and B, respectively) docked onto the receptor binding domain of SARS-CoV-2 S protein (generated by PyMOL program, version 1.7.x). The ligands and the protein are shown as stick and surface, respectively. Panels C and D demonstrate a 2D illustration of the interactions between PM1, PM2 and SARS-CoV-2 S protein (generated by LigPlot program).

the exception of Lys<sup>417</sup> and Gly<sup>496</sup>. Beta, Gamma, and Delta + variants of SARS-CoV-2 have Lys<sup>417</sup> mutation while Gly<sup>496</sup> is mutated in the case of Omicron variant.<sup>[28,30]</sup> According to the possible conformational change induced by some mutations in the binding pocket of spike protein, the interactions of PM1 and PM2 might be influenced. *In silico* and *in vitro* studies of the selected peptidomimetic mole-

cules with different SARS-CoV-2 variants could be of great importance for providing valuable information useful in rationally design of molecules against spike protein of SARS-CoV-2, however it is beyond of this study and could be an interesting topic for future studies.

In this investigation, binding free energy for the peptidomimetic-receptor complexes was calculated. To this

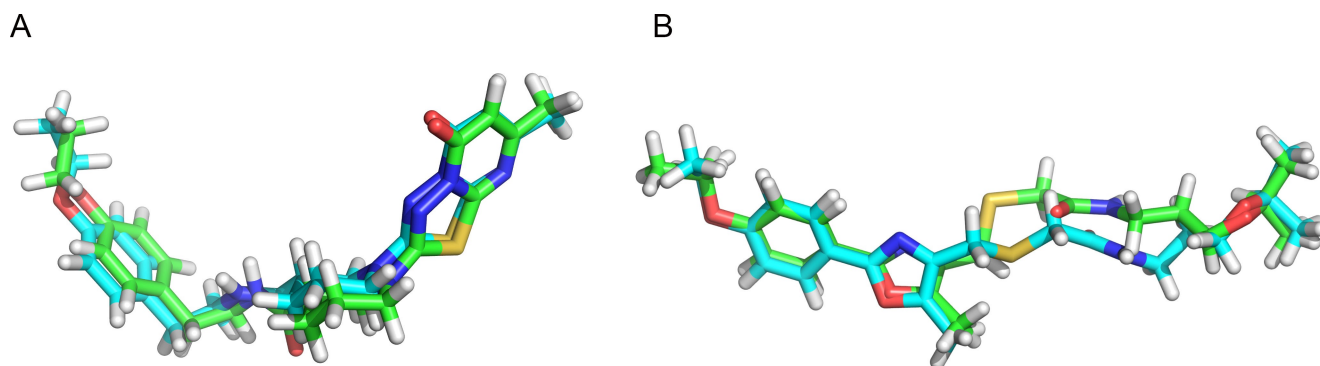


**Figure 3.** Sticks representation of superimposed docking poses of the PM1 (panel A) and PM2 (panel B) bound into the modeled and crystal structures of the spike protein.

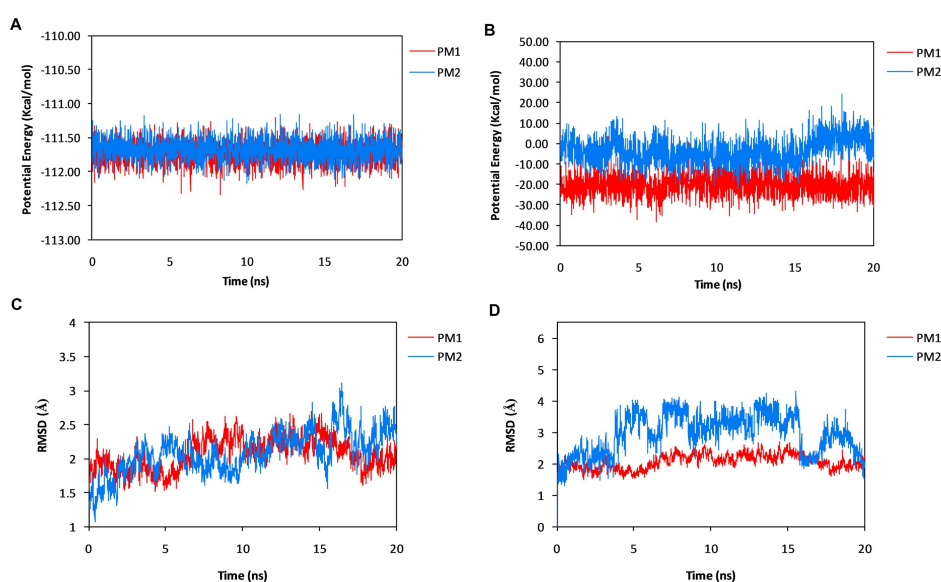


**Figure 4.** The results of molecular dynamics simulation analyses on inhibitor-protein complexes. Panels A and B show the potential energies for the inhibitor-receptor complexes and inhibitors PM1 and PM2 during 20 ns molecular dynamics simulation, respectively. Panels C and D indicate plot of root mean square deviation (RMSD) fluctuation in a 1 to 20 ns molecular dynamics simulation for inhibitor-receptor complexes and inhibitors, respectively.

end, MD simulation of the spike protein in complex with docked peptidomimetics was performed for 20 ns. Analysis of the MD calculations revealed that the complexes were stable and well-equilibrated throughout simulation time inferred from system behavior in terms of potential energies and RMSD (Figure 4). As it can be observed in Figure 4, the potential energy of the systems stays constant during the simulation run time. The RMSD pattern of the trajectories is also indicative of adequate stability of the systems. Table 3 represents binding free energy values ( $\Delta G$ ) calculated for affinity prediction of peptidomimetic compounds to spike protein using MM-PBSA/GBSA algorithms. As the results imply the PM2 compound showed the higher affinity towards spike protein compared to PM1 compound. This is in agreement with experimental findings observed for the

**Table 3.** Calculated mean values of binding free energies for the complex of docked peptidomimetics using Generalized-Born,  $\Delta G_{\text{Binding}}^{\text{(GB)}}$ , and Poisson-Boltzmann,  $\Delta G_{\text{Binding}}^{\text{(PB)}}$  methods for 20 ns MD simulation. Standard deviations are shown in parentheses.

Compound	$\Delta G_{\text{Binding}}^{\text{(GB)}}$	$\Delta G_{\text{Binding}}^{\text{(PB)}}$
PM1	-13.20 ( $\pm$ 7.03)	-12.59 ( $\pm$ 6.04)
PM2	-24.32 ( $\pm$ 4.04)	-18.96 ( $\pm$ 4.34)

peptidomimetic molecules where PM2 revealed some antiviral activity in comparison with PM1. This consistency indicates the reliability of the *in silico* methods in predicting binding affinities of the candidate peptidomimetics to the spike protein of SARS-CoV-2.



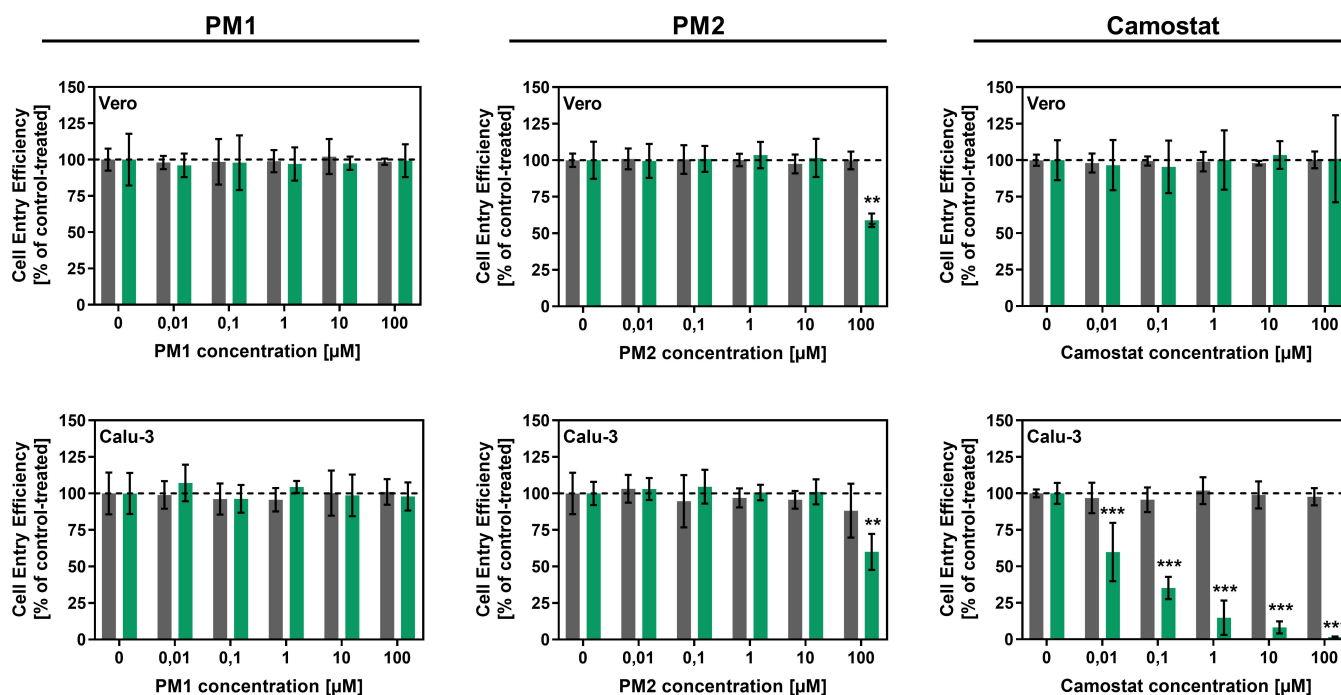


**Figure 5.** Analysis of antiviral activity of PM1 and PM2 against SARS-CoV-2 S protein-driven cell entry. Vero (African green monkey, kidney) or Calu-3 (human, lung) cells were pre-treated with culture medium containing the indicated compound concentrations or DMSO (solvent, control) before being inoculated with pseudotype particles bearing either SARS-CoV-2 S protein (SARS-2-S) or vesicular stomatitis virus glycoprotein (VSV-G). Cells treated with camostat mesylate, a well-known inhibitor of SARS-CoV-2 cell entry into Calu-3 cells, served as a reference. Cell entry of pseudotype particles was analyzed 16 h post inoculation by measuring the activity of virus-encoded luciferase in cell lysates. Presented are the data from a single experiment (performed with three technical replicates) for which entry efficiency was normalized (cell entry in control-treated cells = 100%). Results were confirmed in a second, independent experiment. Error bars indicate the standard deviation. Statistical significance of differences in cell entry between compound- and control-treated cells was analyzed by two-way analysis of variance with Dunnett's post hoc test ( $p > 0.5$  = not significant [not indicated],  $p \leq 0.05$  = \*,  $p \leq 0.01$  = \*\*,  $p \leq 0.005$  = \*\*\*).

In spite of available large amount of marketed therapeutic agents, the need for designing novel pharmaceutical agents is demanding because of prevalence of drug resistance, side effects, as well as inefficiency of available drugs especially for newly emerged disease. In this context, computational approaches have established their own place in rational drug design and discovery process by supplying useful information at the early stages of the pipeline. Due to the costly procedure of drug design and discovery, logical designing of novel therapeutic agent through *in silico* approaches seems necessary which can lead to the reduction of drug candidate failures in clinical trials. There are several reports based on developing antiviral agents<sup>[31]</sup> using such approaches which has become increasingly apparent in the case of SARS-CoV-2.<sup>[32]</sup> Peptidomimetics are a class of therapeutics which benefit the properties of both peptides and small molecules.<sup>[33]</sup> The use of peptidomimetic compounds in virology is not a new approach and a series of anti-viral peptidomimetics are being evaluated in preclinical studies.<sup>[34]</sup> The introduced peptidomimetic compounds in the current study were evaluated in terms of SARS-CoV-2 cell entry using Vero and Calu-3 cell lines and a pseudotype vector surrogate model.

Analysis of the results demonstrated that PM2 exhibits some antiviral activity in both cell lines tested (Figure 5). This effect was specific for particles bearing SARS-CoV-2 S protein as entry for particles bearing VSV-G was not inhibited. However, this antiviral effect was not very strong and required a very high compound concentration of 100  $\mu\text{M}$  (which might be difficult to achieve for treatment of patients). As expected, camostat mesylate, which was used as a reference, inhibited entry of particles bearing SARS-CoV-2 S protein into Calu-3 cells with high efficiency. Although the high concentration of PM2 required for anti-SARS-CoV-2 activity is not favorable for further experimental studies, PM2's structure might serve as scaffold for the design of novel and more powerful SARS-CoV-2 inhibitors following structural optimization through medicinal chemistry-oriented strategies. Evidently, such structural optimization requires rigorous inspection of designed molecules in terms of ADME properties, drug-likeness, and potential toxicity.

## 4 Conclusion

In the current work, we aimed to identify novel peptidomimetic compounds by combining *in silico* and *in vitro* approaches. To this end, a structure-based virtual screening method was employed based on key residues of ACE2 involved in the interaction with SARS-CoV-2 S protein. Following filtering, candidate molecules were selected on the basis of ADME properties, drug-likeness, and toxicity parameters and selected molecules were subjected to molecular docking analysis in order to predict their binding mode towards SARS-CoV-2 S protein. Finally, *in vitro* analysis showed that one of the identified molecules (i.e., PM2) was able to moderately inhibit SARS-CoV-2 S-protein-mediated cell entry. Although the inhibition of cell entry was not strong, the findings of this study may serve as a starting point for structural optimization of the PM2 molecule in order to improve its anti-SARS-CoV-2 activity. Moreover, this study highlights the importance of combining *in silico* and *in vitro* approached in drug discovery, which allows for validation of promising compounds identified through computational simulations and thereby enhances the chances that such compounds will be further investigated in advanced experimental systems (e.g., primary cell culture systems or animal models).

## Acknowledgment

This study was approved at Kurdistan University of Medical Sciences, Sanandaj, Iran (IR.MUK.REC.1398.321). The authors are thankful from Infection Biology Unit, German Primate Center – Leibniz Institute for Primate Research, Göttingen, Germany, for experimental facilities.

## Conflict of interest

None declared.

## Data Availability Statement

Data available on request from the authors.

## References

- [1] a) N. Zhu, D. Zhang, W. Wang, X. Li, B. Yang, J. Song, X. Zhao, B. Huang, W. Shi, R. Lu, P. Niu, F. Zhan, X. Ma, D. Wang, W. Xu, G. Wu, G. F. Gao, W. Tan, *N. Engl. J. Med.* **2020**, *382*, 727–733; b) P. Zhou, X. L. Yang, X. G. Wang, B. Hu, L. Zhang, W. Zhang, H. R. Si, Y. Zhu, B. Li, C. L. Huang, H. D. Chen, J. Chen, Y. Luo, H. Guo, R. D. Jiang, M. Q. Liu, Y. Chen, X. R. Shen, X. Wang, X. S. Zheng, K. Zhao, Q. J. Chen, F. Deng, L. L. Liu, B. Yan, F. X. Zhan, Y. Y. Wang, G. F. Xiao, Z. L. Shi, *Nature* **2020**, *579*, 270–273.
- [2] T. M. Abd El-Aziz, J. D. Stockand, *Infect. Genet. Evol.* **2020**, *83*, 104327.
- [3] M. Pal, G. Berhanu, C. Desalegn, V. Kandi, *Cureus* **2020**, *12*, e7423.
- [4] a) L. Wang, Y. Wang, D. Ye, Q. Liu, *Int. J. Antimicrob. Agents* **2020**, *55*, 105948; b) N. van Doremalen, T. Bushmaker, D. H. Morris, M. G. Holbrook, A. Gamble, B. N. Williamson, A. Tamin, J. L. Harcourt, N. J. Thornburg, S. I. Gerber, J. O. Lloyd-Smith, E. de Wit, V. J. Munster, *N. Engl. J. Med.* **2020**, *382*, 1564–1567; c) J. L. Santarpia, D. N. Rivera, V. L. Herrera, M. J. Morwitzer, H. M. Creager, G. W. Santarpia, K. K. Crown, D. M. Brett-Major, E. R. Schnaubelt, M. J. Broadhurst, J. V. Lawler, S. P. Reid, J. J. Lowe, *Sci. Rep.* **2020**, *10*, 12732.
- [5] a) K. Diriba, E. Awulachew, E. Getu, *Eur. J. Med. Res.* **2020**, *25*, 39; b) M. Maqsood, Y. Karim, E. Fatima, S. Marriam, R. Afzal, *Biomed. Lett.* **2020**, *6*, —149–163; c) S. Gupta, J. Parker, S. Smits, J. Underwood, S. Dolwani, *Colorectal Dis* **2020**, *22*, 611–620.
- [6] a) F. Jiang, L. Deng, L. Zhang, Y. Cai, C. W. Cheung, Z. Xia, *J. Gen. Intern. Med.* **2020**, *35*, 1545–1549; b) A. Gupta, M. V. Madhavan, K. Sehgal, N. Nair, S. Mahajan, T. S. Sehrawat, B. Bikdeli, N. Ahluwalia, J. C. Ausiello, E. Y. Wan, D. E. Freedberg, A. J. Kirtane, S. A. Parikh, M. S. Maurer, A. S. Nordvig, D. Accili, J. M. Bathon, S. Mohan, K. A. Bauer, M. B. Leon, H. M. Krumholz, N. Uriel, M. R. Mehra, M. S. V. Elkind, G. W. Stone, A. Schwartz, D. D. Ho, J. P. Bilezikian, D. W. Landry, *Nat. Med.* **2020**, *26*, 1017–1032.
- [7] A. Kronbichler, D. Kresse, S. Yoon, K. H. Lee, M. Effenberger, J. I. Shin, *Int. J. Infect. Dis.* **2020**, *98*, 180–186.
- [8] J. M. Sanders, M. L. Monogue, T. Z. Jodlowski, J. B. Cutrell, *Jama* **2020**, *323*, 1824–1836.
- [9] a) S. Choudhary, Y. S. Malik, S. Tomar, *Front. Immunol.* **2020**, *11*, 1664; b) A. Trezza, D. Iovinelli, A. Santucci, F. Prisch, O. Spiga, *Sci. Rep.* **2020**, *10*, 13866; c) B. Br. H. Damle, S. Ganju, L. Damle, *F1000Research* **2020**, *9*, 663; d) S. Unni, S. Aouti, S. Thiyagarajan, B. Padmanabhan, *J. Biosci.* **2020**, *45*.
- [10] a) A. C. Walls, Y. J. Park, M. A. Tortorici, A. Wall, A. T. McGuire, D. Velesler, *Cell* **2020**, *183*, 1735; b) X. Xia, *Viruses* **2021**, *13*.
- [11] a) J. Lan, J. Ge, J. Yu, S. Shan, H. Zhou, S. Fan, Q. Zhang, X. Shi, Q. Wang, L. Zhang, X. Wang, *Nature* **2020**, *581*, 215–220; b) J. Yang, S. J. L. Petitjean, M. Koehler, Q. Zhang, A. C. Dumitru, W. Chen, S. Derclay, S. P. Vincent, P. Soumillion, D. Alsteens, *Nat. Commun.* **2020**, *11*, 4541.
- [12] Y. Wan, J. Shang, R. Graham, R. S. Baric, F. Li, *J. Virol.* **2020**, *94*.
- [13] M. Floris, J. Masciocchi, M. Fanton, S. Moro, *Nucleic Acids Res.* **2011**, *39*, W261–269.
- [14] A. Daina, O. Michielin, V. Zoete, *Sci. Rep.* **2017**, *7*, 42717.
- [15] a) C. A. Lipinski, F. Lombardo, B. W. Dominy, P. J. Feeney, *Adv. Drug Delivery Rev.* **2001**, *46*, 3–26; b) D. F. Veber, S. R. Johnson, H. Y. Cheng, B. R. Smith, K. W. Ward, K. D. Kopple, *J. Med. Chem.* **2002**, *45*, 2615–2623; c) A. K. Ghose, V. N. Viswanadhan, J. J. Wendoloski, *J. Comb. Chem.* **1999**, *1*, 55–68; d) I. Muegge, S. L. Heald, D. Brittelli, *J. Med. Chem.* **2001**, *44*, 1841–1846; e) W. J. Egan, K. M. Merz, Jr., J. J. Baldwin, *J. Med. Chem.* **2000**, *43*, 3867–3877.
- [16] a) A. Vedani, M. Dobler, Z. Hu, M. Smieško, *Toxicol. Lett.* **2015**, *232*, 519–532; b) A. Vedani, M. Dobler, M. Smieško, *Toxicol. Appl. Pharmacol.* **2012**, *261*, 142–153.
- [17] M. Froimowitz, *BioTechniques* **1993**, *14*, 1010–1013.
- [18] M. L. Verdonk, J. C. Cole, M. J. Hartshorn, C. W. Murray, R. D. Taylor, *Proteins* **2003**, *52*, 609–623.

- [19] a) W. L. DeLano, *CCP4 Newsletter on protein crystallography* **2002**, *40*, 82–92; b) A. C. Wallace, R. A. Laskowski, J. M. Thornton, *Protein Eng.* **1995**, *8*, 127–134.
- [20] a) D. A. Pearlman, D. A. Case, J. W. Caldwell, W. S. Ross, T. E. Cheatham, S. DeBolt, D. Ferguson, G. Seibel, P. Kollman, *Comput. Phys. Commun.* **1995**, *91*, 1–41; b) D. A. Case, T. E. Cheatham, 3rd, T. Darden, H. Gohlke, R. Luo, K. M. Merz, Jr., A. Onufriev, C. Simmerling, B. Wang, R. J. Woods, *J. Comput. Chem.* **2005**, *26*, 1668–1688.
- [21] P. A. Kollman, I. Massova, C. Reyes, B. Kuhn, S. Huo, L. Chong, M. Lee, T. Lee, Y. Duan, W. Wang, O. Donini, P. Cieplak, J. Srinivasan, D. A. Case, T. E. Cheatham, *Acc. Chem. Res.* **2000**, *33*, 889–897.
- [22] J. Weiser, P. S. Shenkin, W. C. Still, *J. Comput. Chem.* **1999**, *20*, 217–230.
- [23] a) M. Hoffmann, H. Hofmann-Winkler, J. C. Smith, N. Krüger, P. Arora, L. K. Sørensen, O. S. Søgaard, J. B. Hasselstrøm, M. Winkler, T. Hempel, L. Raich, S. Olsson, O. Danov, D. Jonigk, T. Yamazoe, K. Yamatsuta, H. Mizuno, S. Ludwig, F. Noé, M. Kjolby, A. Braun, J. M. Sheltzer, S. Pöhlmann, *e-biomed* **2021**, *65*, 103255; b) M. Hoffmann, H. Kleine-Weber, S. Schroeder, N. Krüger, T. Herrler, S. Erichsen, T. S. Schiergens, G. Herrler, N. H. Wu, A. Nitsche, M. A. Müller, C. Drosten, S. Pöhlmann, *Cell* **2020**, *181*, 271–280.e278.
- [24] a) M. Berger Rentsch, G. Zimmer, *PLoS One* **2011**, *6*, e25858; b) H. Kleine-Weber, M. T. Elzayat, L. Wang, B. S. Graham, M. A. Müller, C. Drosten, S. Pöhlmann, M. Hoffmann, *J. Virol.* **2019**, *93*.
- [25] C. Contini, M. Di Nuzzo, N. Barp, A. Bonazza, R. De Giorgio, M. Tognon, S. Rubino, *J. Infect. Dev. Ctries.* **2020**, *14*, 254–264.
- [26] J. Xiong, Y. Xiang, Z. Huang, X. Liu, M. Wang, G. Ge, H. Chen, J. Xu, M. Zheng, L. Chen, *Front. Chem.* **2021**, *9*, 740702.
- [27] A. E. Farouk, M. H. Baig, M. I. Khan, T. Park, S. S. Alotaibi, J. J. Dong, *Saudi J. Biol. Sci.* **2021**, *28*, 3262–3269.
- [28] S. Rajpoot, K. Solanki, A. Kumar, K. Y. J. Zhang, S. S. Pullamsetti, R. Savai, S. M. Faisal, Q. Pan, M. S. Baig, *Int. J. Pept. Res. Ther.* **2021**, *28*, 28.
- [29] A. Acharya, K. Pandey, M. Thurman, E. Klug, J. Trivedi, K. Sharma, C. L. Lorson, K. Singh, S. N. Byrareddy, *J. Virol.* **2021**, *95*, e0143721.
- [30] S. R. Kannan, A. N. Spratt, K. Sharma, H. S. Chand, S. N. Byrareddy, K. Singh, *J. Autoimmune Dis.* **2022**, *126*, 102779.
- [31] a) J. Vora, S. Patel, S. Sinha, S. Sharma, A. Srivastava, M. Chhabria, N. Shrivastava, *J. Biomol. Struct. Dyn.* **2019**, *37*, 131–146; b) S. Mathew, A. A. Al Thani, H. M. Yassine, *PLoS One* **2018**, *13*, e0203148; c) S. Mathew, S. Taleb, A. H. Eid, A. A. Althani, H. M. Yassine, *Emergent. Mater.* **2021**, 1–11.
- [32] a) A. Francés-Monerris, C. Hognon, T. Miclot, C. García-Iriepa, I. Iriepa, A. Terenzi, S. Grandemange, G. Barone, M. Marazzi, A. Monari, *J. Proteome Res.* **2020**, *19*, 4291–4315; b) F. Hufsky, K. Lamkiewicz, A. Almeida, A. Aouacheria, C. Arighi, A. Bateman, J. Baumbach, N. Beerenwinkel, C. Brandt, M. Cacciabue, S. Chuguransky, O. Drechsel, R. D. Finn, A. Fritz, S. Fuchs, G. Hattab, A. C. Hauschild, D. Heider, M. Hoffmann, M. Hölzer, S. Hoops, L. Kaderali, I. Kalvari, M. von Kleist, R. Kmiecinski, D. Kühnert, G. Lasso, P. Libin, M. List, H. F. Löchel, M. J. Martin, R. Martin, J. Matschinske, A. C. McHardy, P. Mendes, J. Mistry, V. Navratil, E. P. Nawrocki, N. O'Toole, Á. N. Ontiveros-Palacios, A. I. Petrov, G. Rangel-Pineros, N. Redaschi, S. Reimering, K. Reinert, A. Reyes, L. Richardson, D. L. Robertson, S. Sadegh, J. B. Singer, K. Theys, C. Upton, M. Welzel, L. Williams, M. Marz, *Briefings Bioinf.* **2021**, *22*, 642–663.
- [33] G. Zhang, J. Andersen, G. Gerona-Navarro, *Protein Pept. Lett.* **2018**, *25*, 1076–1089.
- [34] a) F. Amblard, S. Zhou, P. Liu, J. Yoon, B. Cox, K. Muzzarelli, B. D. Kuiper, L. C. Kovari, R. F. Schinazi, *Bioorg. Med. Chem. Lett.* **2018**, *28*, 2165–2170; b) S. VanPatten, M. He, A. Altiti, F. C. K. M. H. Ghanem, Y. Al-Abed, *Future Med. Chem.* **2020**, *12*, 1647–1656.

Received: January 12, 2022

Accepted: January 16, 2022

Published online on February 1, 2022